Available online at www.sciencedirect.com
SCIENCE DIRECT®
Physics of the Earth and Planetary Interiors 156 (2006) 223–241
PHYSICS OF THE EARTH AND PLANETARY INTERIORS
www.elsevier.com/locate/pepi

Long-term trends in paleointensity: The contribution of DSDP/ODP submarine basaltic glass collections

Lisa Tauxe*

Scripps Institution of Oceanography, USA

Received 9 August 2004; received in revised form 17 February 2005; accepted 25 March 2005

Abstract

The Deep Sea Drilling Project and the Ocean Drilling Program have been collecting fresh appearing submarine basaltic glass from the world's oceans for over three decades. This glass has proved nearly ideal for estimating paleointensity variations of the Earth's magnetic field. We compile here data for 726 paleointensity experiments from six publications on paleointensity using DSDP/ODP glass. We also include new data for an additional 225 specimens. These were obtained through the so-called "IZZI" paleointensity experiment of [Tauxe, L., Staudigel, H., 2004. Strength of the geomagnetic field in the cretaceous normal superchron: new data from submarine basaltic glass of the troodos ophiolite. Geochem. Geophys. Geosyst. 5 (2), Q02H06, doi:10.1029/2003GC000635] whereby infield-zerofield steps are alternated with the zerofield-infield steps to enhance quality assessment of the resulting data. The entire collection of data from 951 experiments was prepared for uploading to the MagIC data base (http://earthref.org), including original measurements, interpretations, and useful metadata. Excellent results were obtained throughout the depth (> 1400 mbsf) and age (0–160 Ma) range sampled. DSDP/ODP glass data are compared with published paleointensity data meeting minimal acceptance criteria from the time interval 1–160 Ma. Paleolatitudes were estimated for all cooling units in a self-consistent manner for use in calculating virtual axial dipole moments. We conclude: (1) There is about a 20% difference in mean values between the SBG and the lava flow data (48 ± 36 and 57 ± 29 ZAm^2 respectively). The difference is caused by the fact that there are more higher values in the lava flow data than in the SBG data set rather than a difference in the minimum values. Lava flows cooling over a periods of days to months can account for the discrepancy. (2) The positive relationship between polarity interval length and average paleofield intensity first hypothesized by [Cox, A.V., 1968. Lengths of geomagnetic polarity intervals. J. Geophys. Res. 73, 3247–3260] is supported by data compiled here. The Brunhes data (for which we have only a minimum estimate for polarity interval length) are consistent with a long polarity interval, suggesting that instead of racing toward reversal [Hulot, G., Eymin, C., Langlais, B., Mandea, M., Olsen, N., 2002. Small-scale structure of the geodynamo inferred from oersted and magsat satellite data. Nature 416, 620–623], we could instead be in the midst of a long stable polarity interval. (3) Because the average value appears to be a function of polarity interval length, it is probably not useful to calculate a mean value. Nonetheless, it appears that most of the time (apart from the Brunhes and the longest polarity intervals), the average dipole moment is substantially less than the present day value as suggested by [Juarez, T., Tauxe, L., Gee, J.S., Pick, T., 1998. The intensity of the earth's magnetic field over the past 160 million years. Nature 394, 878–881].

Keywords: DSDP and ODP; Paleointensity; Submarine basaltic glass; Paleomagnetism; The IZZI method; Thellier-Thellier experiments

1. Introduction

The present Earth's magnetic field is well approximated by a geocentric magnetic dipole with a moment

* Tel.: +1 858 534 6084; fax: +1 858 534 0784.
E-mail address: ltauxe@ucsd.edu (L. Tauxe)

0031-9201/$ – see front matter © 2006 Published by Elsevier B.V.
doi:10.1016/j.pepi.2005.03.022

of about 80 ZAm^2 ["Z" stands for Zetta (10^{21})]. According to recent analyses of the magnetic field from satellite observations, the strength of the magnetic field is dropping rapidly, leading some to speculate that we are approaching a polarity reversal (e.g., Hulot et al., 2002). The likelihood of this scenario depends on a critical view of the history of the intensity of the magnetic field. What is the average value of the dipole moment? What is its variation in times of stable polarity? Moreover, as asked by Coe (1967b) "How low has the intensity fallen without subsequent reversal?", and "Has there been a general trend of the geomagnetic intensity through geologic time?" Answers to these questions require a large collection of reliable paleointensity data that span a significant period of time.

A great deal of effort has been put into assembling paleointensity databases over more than three decades. Yet there remains little consensus on the answers to the most basic questions. Early studies focussing on averages of the so-called virtual dipole moments (VDMs, or the dipole moment required to produce the observed field strength at the magnetic latitude of the observation site) suggested that the average field strength has either been quite a bit lower than the present (e.g., Smith, 1967 and Coe, 1967b) or approximately equivalent to today's field (Kono, 1971; Bol'shakov and Solodovnikov, 1980, and McFadden and McElhinny, 1982). Some studies found no trend with age in VDMs (e.g., Bol'shakov and Solodovnikov, 1980) over the last few hundred million years, while others found a significant increase in dipole moment from the Mesozoic toward the present (e.g., Smith, 1967).

Even as the paleointensity database has grown, the arguments have continued. For example, Tanaka et al. (1995) estimated the average dipole moment for the last 20 Myr to be approximately 84 ZAm^2 with significantly lower values in the Mesozoic (the so-called "Mesozoic Dipole Low" of Prévot et al., 1990), a view also held by Perrin and Shcherbakov (1997) and recently reiterated by Biggin and Thomas (2003). But Juarez et al. (1998), Juarez and Tauxe (2000) and Selkin and Tauxe (2000) argued for a lower average dipole moment of some 45 or 50 ZAm^2 implying that the Mesozoic Dipole Low was not "low" but was of average paleomagnetic intensity.

The lack of consensus on such basic questions as to what the average field is and whether there are any trends over time stems from differing views on the data selection (see e.g., Selkin and Tauxe, 2000; Heller et al., 2002; Biggin and Thomas, 2003, and Goguitchaichvili et al., 2004). For example (e.g., Biggin and Thomas, 2003) argue that because such procedures as the so-called "pTRM check" designed to identify alteration during the paleointensity experiment (see, e.g., Coe, 1967a) cannot guarantee the quality of the result, there is no need to reject data that do not have pTRM checks. In contrast, others (e.g., Riisager and Riisager, 2001 and Tauxe and Staudigel, 2004) have developed more rigorous experimental protocols to detect and reject "bad" data.

What everyone agrees on is that more and better data would be helpful for defining the average paleofield intensity and its variation. The dearth of reliable paleointensity derives from the difficulty of finding suitable material and the time consuming nature modern paleointensity experiments.

Paleointensity experiments require that the carrier of magnetic remanence be sufficiently small that the blocking and unblocking temperatures are the same. Moreover, the cooling rate must be similar in the lab as it was during original cooling, or there must be cooling rate correction (e.g., Fox and Aitken, 1980). Finally, the magnetic phase may not change its capacity to acquire a thermal remanence during the experiment. Submarine basaltic glass (SBG), formed during the quenching of the lava in seawater, often meets these requirements (e.g., Pick and Tauxe, 1993b; Mejia et al., 1996; Carlut and Kent, 2000; Selkin and Tauxe, 2000; Tauxe and Staudigel, 2004; Bowles et al., 2005).

Ocean basins cover a large area of the Earth's surface, and marine magnetic anomalies provide tight age constraints at many drill sites. Therefore Deep Sea Drilling Project (DSDP) and the Ocean Drilling Program (ODP) submarine basaltic glass is a valuable resource for studies of palaeointensity. The drilling programs obtained samples from over 60 sites that recovered reasonably fresh looking volcanic glass with magnetizations sufficient for paleomagnetic study (chips with natural remanent moments of ≥ 1 nAm^2) (see Fig. 1 and Table 1). These glasses have been the subject of paleointensity study for over a decade (Pick and Tauxe, 1993b,a, 1994; Juarez et al., 1998; Juarez and Tauxe, 2000; Selkin and Tauxe, 2000; Smirnov and Tarduno, 2003; Riisager et al., 2003).

The reliability of submarine basaltic glass paleointensities has been questioned because the magnetization is carried by low-titanium magnetite which is not an equilibrium phase in mid-ocean ridge basalts (see, e.g., Heller et al., 2002). Glass is not an equilibrium phase so the equilibrium phase of TM60 (titanium substituted for 60% of the iron) is not necessarily expected. In fact, iron is more mobile than titanium in the melt and lower titanium magnetites are therefore more likely in the rapidly quenched glass phase.

Tauxe and Staudigel (2004) summarized the evidence that the glassy rinds of submarine pillow basalts and

Table 1
Locations, ages, and paleolatitude informtion for the DSDP/ODP sites referred to in this study

Site	λ	ϕ	Age (Ma)	Age Uncert.	Age meth.	Ref.	λ'	Plate	Ref.
169	11	174	148	2	M21	[1,2]	−27.9	PA	[5]
205	−25	178	30.7	0.5	C12n	[3]	−36	FB	[6]
238	−11	71	32	2	(P19)	[3]	−25	IN	[7]
322	−60	−79	48	2	C21–C22	[3]	−62	ANT	[7]
332	37	−34	3.6	0.1	C2Ar	[3]	37	NA	[7]
334	37	−34	9.8	0.5	C5n.1n	[3]	32	NA	[7]
335	37	−35	13.8	2	C5A-C5B	[3]	31	NA	[7]
395	23	−46	8	1	C4n	[3]	18	NA	[7]
396	22.5	−43.5	10.3	0.5	C5n	[3]	18	AF	[7]
407	64	−31	33.3	0.1	C13n	[3]	54	NA	[7]
410	46	−30	10.3	0.7	C5n	[3]	41	NA	[7]
417	25	−68	121	1	M0	[3]	20	NA	[7]
418	25	−68	121	1	M0	[3]	20	NA	[7]
420	9	−106	3.4	0.2	C2A	[3]	9	PA	[13]
423	9	−105	1.7	0.2	C2	[3]	9	PA	[13]
447	18	133	43	2	C20	[3]	26	EU	[6]
448	16	135	31	1	(NP23)	[3]	23	EU	[6]
456	18	145	3.7	0.2	C2Ar	[3]	18	PA	[13]
458	18	147	32	1	(WPN-15)	[3]	4	PA	[14]
462	7	165	111	1	$^{40}Ar/^{39}Ar$	[4]	−33	PA	[8]
469	33	−121	18.7	0.2	C5E	[3]	34	NA	[7]
470	29	−118	15.2	0.5	C5B	[3]	29	NA	[7]
472	23	−114	16	1		[3]	17	PA	[13]
474	23	−109	3.1	0.2	C2A	[3]	23	NA	[13]
482	23	−108	0.3	0.3	C1	[3]	23	NA	[13]
483	23	−108	2	0.2	C2-C2A	[3]	23	NA	[13]
495	12.5	−91	20.7	0.2	C6a	[3]	2.5	CO	[12]
504	1	−84	7.25	0.2	C3B	[3]	1	NZ	[12]
510	2	−86	3.1	0.4	C2A	[3]	2	CO	[13]
520	−26	−11	15.2	0.2	C5Br	[3]	−34	AF	[7]
522	−27	−5	35.7	1.3	C16n	[3]	−39	AF	[7]
525	−29	3	72	1	C32n	[2]	−39	AF	[7]
530	−19	9	97	5	(l Alb.- e. Cen.)	[2]	−26	AF	[7]
534	28	−75	156.5	0.1	M28	[2]	16	NA	[7]
543	16	−59	84	1	C34n/C34r	[2]	18	NA	[7]
556	39	−35	30.7	0.2	C12n	[3]	30	NA	[7]
558	38	−37	34	0.5	C13r	[3]	29	NA	[7]
559	35	−41	32	1.1	C12r	[3]	26	NA	[7]
562	33	−42	17.4	0.2	C5Dn	[3]	24	NA	[7]
563	34	−44	33.2	0.1	C13n	[3]	26	NA	[7]
564	34	−44	33.2	0.1	C13n	[3]	26	NA	[7]
572	1	−114	15	0.2	(N9)	[3]	−5	PA	[14]
573	0	−133	34.5	0.5	(P16)	[3]	−13.1	PA	[14]
706	−13	61	82	2	(e Camp.)	[2]	−35	AF	[7]
758	5	90	155.7	0.3	M26	[2]	−51	IN	[7]
765	−16	118	155.7	0.3	M26	[2]	−39	AU	[7]
770	5	124	38.9	1	(P14)	[3]	14	EU	[6]
781	20	147	2.6	0.1	(CN12b)	[3]	20	PA	[13]
801	19	156	164.4	3	(l Bath. - e Berri.)	[2]	−9	PA	[9]
802	12	153	114.6	3.2	(CC9)	[2]	−19.4	PA	[9]
803	2	161	88	6	$^{40}Ar/^{39}Ar$	[11]	−32	PA	[10]
807	4	157	122.4	0.8	$^{40}Ar/^{39}Ar$	[11]	−34	PA	[10]
833	15	168	4.5	0.5	(N19)	[3]	15	PA	[13]
834	−19	−178	6	0.2	C3A	[3]	−19	LB	[13]
835	−19	−177	2.8	1	(CN12)	[3]	−19	LB	[13]
836	−20	−177	1	0.3	(C14a)	[3]	−20	LB	[13]
843	19	−159	97	5	(l Alb.- e. Cen.)	[2]	−16	PA	
862	−47	−76	2.8	1	(NN16−18)	[3]	−47	SA	[13]

Table 1 (*Continued*)

Site	λ	ϕ	Age (Ma)	Age Uncert.	Age meth.	Ref.	λ'	Plate	Ref.
864	10	−104	0	0.1	“zero-age”		10	EPR	[13]
907	69	−13	0	1	(C6)	[3]	69	EU	[13]
1001	16	−76	77.6	3.8	(CC21)	[2]	23	NA	[7]

Biostratigraphic constraints are in parentheses. [1] Nakanishi et al. (1992); [2] Gradstein et al. (1995); [3] Berggren et al. (1995); [4] Castillo et al. (1994); [5] Sager (2004); [6] Lee and Lawver (1995): reconstructed to stable Europe, λ' here used Besse and Courtillot (2002) for EU; [7] Besse and Courtillot (2002); [8] Steiner (1981); [9] Wallick and Steiner (1992); [10] Yan and Kroenke (1993); [11] Mahoney et al. (1993); [12] DeMets et al. (1990); [13] present latitude; [14] 0.4°/Myr. PA: Pacific; FB: Fiji Basin; IN: Indian; ANT: Antarctic; NA: North American; AF: African; EU: European; CO: Cocos; NZ: Nazca; LB: Lau Basin; SA: South American; EPR: East Pacific Rise (Axial Summit Caldera); l Alb.- e. Cen.: late Albian to early Cenomenian; e Camp: early Campanian; l Bath. - e Berri.: late Bathonian to early; Berriasian; WPN-15 (lower NP23).

sheet flows are excellent materials for paleointensity experiments. Briefly, rock magnetic studies suggest that low-Ti single-domain titanomagnetite carries the remanent magnetization in both ancient glasses and those obtained from dredges of flows extruded within a few months of sampling (e.g., Pick and Tauxe, 1994; Carlut and Kent, 2000). Magnetite grows at elevated temperatures (Pick and Tauxe, 1994; Smirnov and Tarduno, 2003), but not at 2 °C on the sea floor; hence the low-Ti magnetite that is present in even zero-age pillow margin glass must have formed during quenching. Indeed, it appears that only the large opaque oxides seen in thin section have the ideal titanomagnetite composition with $x = 0.6$. Titanomagnetites in interstitial glass show a surprising range of titanium substitution $0 < x < 0.8$ (Zhou et al., 1997). Moreover, paleointensity experiments on basaltic glass from sites of recent eruptions recover the ambient magnetic field at those locations (Pick and Tauxe, 1993b,a; Kent and Gee, 1996; Carlut and Kent, 2000). Therefore, the evidence suggests overwhelmingly that the remanence was acquired during quenching, that SBG can evade alteration for geologically significant periods of time and that it frequently behaves in an ideal fashion during the paleointensity experiment. Finally, a new study by Bowles et al. (2005) shows that by happy coincidence, the cooling rate of submarine basaltic glass during its initial quenching is quite well reproduced in our laboratory. It is the purpose of this paper to compile published and new data from Thellier–Thellier experiments (at least with pTRM checks) including data from submarine basaltic glass from DSDP/ODP material.

2. Materials and methods

In this paper, we assemble all the measurement data from 726 specimens from Pick and Tauxe (1993b,a, 1994), Juarez et al. (1998), Juarez and Tauxe (2000), and Selkin and Tauxe (2000). Details of sampling sites

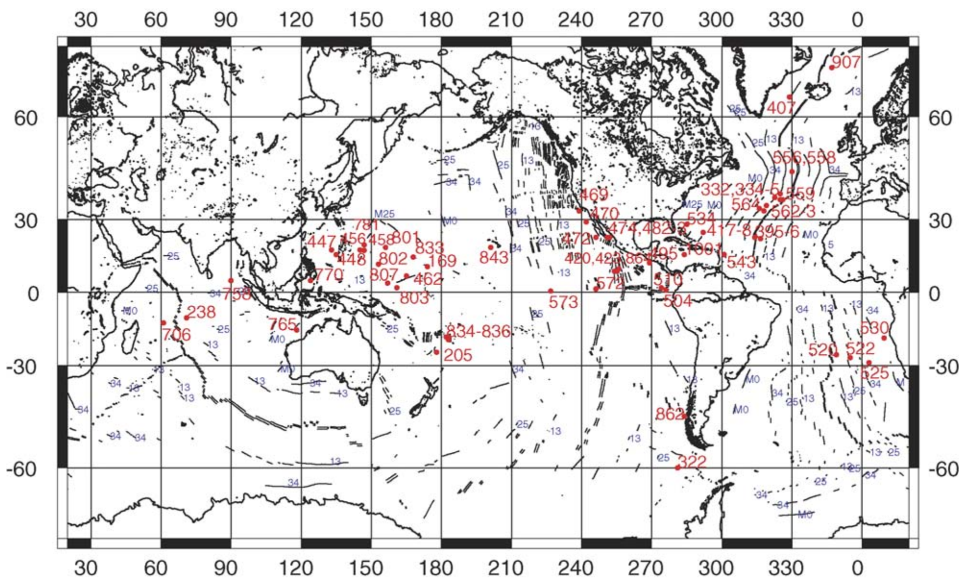

Fig. 1. Map of DSDP/ODP drill sites for samples discussed in this paper. Also shown are selected magnetic anomalies from Cande et al. (1989). See Table 1 for details.

are summarized in Table 1 and the locations are shown in Fig. 1. Please note that every age constraint in Table 1 was verified with the most recent available information. We have relied on the time scales of Berggren et al. (1995) or Gradstein et al. (1995) to convert magnetic anomalies and biostratigraphic age constraints to absolute ages. The uncertainties in Table 1 are in most cases best guesses as to the possible age range based on the available information.

Experimental design has evolved substantially from the first study of Pick and Tauxe (1993a). Relevant parameters such as laboratory field strength, etc., are tabulated in template files compatible with the MagIC database. In our early studies, only eight specimens could be run in a single heating/cooling step. Therefore, the original studies often had single specimens from a given quenched margin. In our most recent experiments we run up to 60 specimens in a single heating and cooling step, meaning that we can complete a full paleointensity experiment on over 100 specimens in less than a month. In order to augment the published data, in particular to obtain replicate specimens from promising samples, we selected an additional 225 specimens from available glass material from 23 DSDP/ODP sites for new paleointensity experiments. These were prepared in the manner described by Tauxe and Staudigel (2004).

Specimens selected for the present study were subjected to the modified Thellier–Thellier (Thellier and Thellier, 1959) experimental protocol known as the "IZZI experiment" (Tauxe and Staudigel, 2004) described briefly here (see Fig. 2a). Specimens were heated to 100 °C and cooled in zerofield. After measuring the natural remanent magnetization (NRM), the specimens were re-heated to 100 °C, cooled in a laboratory field of 40 μT directed along the specimen's "Z" axis and remeasured. The difference in the *Z* component between the second step and the first is the partial thermal remanence (pTRM) gained by cooling from 100 °C to room

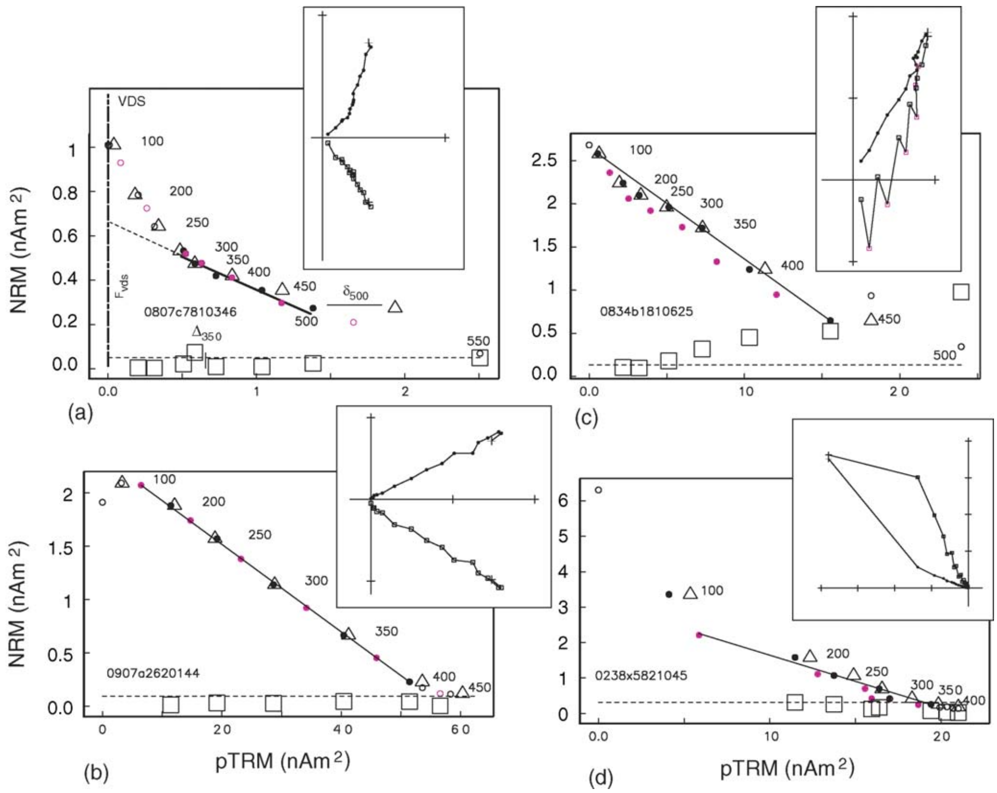

Fig. 2. Representative results from the IZZI experiment described in the text (see also Table 2). Circles are the NRM remaining versus pTRM gained at each temperature step. Darker (lighter) symbols are the ZI (IZ) steps. (Open) closed symbols are (excluded) included in the slope calculation. Triangles are the pTRM checks and squares are the pTRM-tail checks. Solid lines connect the highest and lowest data points used in the calculation and are not the "best-fit" lines. Insets are vector end-point diagrams of the zero-field steps. (a) The total remanence estimated by summing the vector difference between subsequent demagnetization steps (VDS) the dash-dot line. The fraction F_{vds} is the portion of the VDS used in the paleointensity calculation. δ_i and Δ_i are the pTRM checks and pTRM tail checks. (b) Example of nearly ideal behavior. (c) Example of the zig–zag behavior detected in the IZZI experiment when blocking and unblocking temperatures are not the same. (d) Example of experimental data that barely meet acceptance criteria.

temperature. This zero-field, in-field (or ZI) heating procedure was alternated with an in-field, zero-field (or IZ) step whereby samples are first heated and cooled in the laboratory field and measured, then heated and cooled in zero-field and measured. The IZ steps are represented by lighter colored symbols in Fig. 2. At each ZI step (darker colored symbols), there are two additional steps. One is a reheating to a lower temperature step and cooling in the laboratory field done between the zero-field and the in-field steps. The pTRM gained in this repeated step (the so-called pTRM check of, for example, Coe et al. (1978)), is compared with the first in field step at the same temperature. A difference (e.g., δ_{500} in Fig. 2a) is an indication of a change in the capacity of the specimen to acquire pTRM. A second additional step is inserted after the ZI steps, whereby the specimens are heated for a third time to the same temperature and cooled in zero-field. This so-called pTRM tail check step (e.g., Riisager and Riisager, 2001) is used to test if the pTRM gained when cooling in the lab field is entirely removed by reheating to the same temperature step, a necessary condition for reliable paleointensity determinations. A difference (e.g., (Δ_{350} in Fig. 2a)) is indicative of a failure of the blocking and unblocking reciprocity requirement (although it can also be accompanied by a large δ_i suggesting alteration).

Fig. 2b is an example of the behavior of the best submarine basaltic glass specimens during the IZZI experiment. Data from IZ (darker symbols) and ZI (lighter symbols) steps fall along a single line in the NRM–pTRM plots. The pTRM checks (triangles) generally overlie the original measurements. The zero-field steps produce vector end-point diagrams (inset) that have well determined, single component directions that trend to the origin. Finally, the pTRM-tail check steps (squares) indicate that any pTRM acquired at a given temperature is completely removed by heating to the same temperature and cooling in zero-field.

In certain specimens, the IZZI protocol leads to rather interesting behavior, explained in detail by Yu et al. (2004). The data in Fig. 2c with pTRM checks (associated with triangles) are the zero-field-infield (ZI) steps (darker circles) and the intervening steps are the infield-zero-field (IZ) steps (lighter circles, squares in inset). Alternating the two procedures can result in a "zigzag" in the NRM-pTRM plots and/or the vector end-point diagrams (see inset). This "zig-zagging" is reflected in larger scatter about the best fit line in both the NRM-pTRM plots and the vector end-point diagrams and is generally accompanied by large values of Δ, particularly in the intermediate blocking temperature interval. The failure of the principle assumptions of the Thellier–Thellier method would not necessarily be apparent in experiments without at least the pTRM tail checks because the IZ steps line up very well in the NRM-pTRM plots. The zig-zagging is a direct consequence of non-reciprocity of blocking and unblocking temperature steps which also is reflected in the pTRM tail checks. We note that the IZZI protocol renders the pTRM tail checks redundant, thus potentially saving time while not sacrificing any information on data reliability.

The reliability of paleointensity data can be judged in a number of ways. There are many parameters in the lit-

Table 2
Parameters

Parameter	Name	Definition/notes	Ref.
$\lvert b\rvert$	Best-fit slope	Slope of pTRM acquired versus NRM remaining	[1]
$B_{\rm anc}$	Ancient field estimate	$\lvert b\rvert$ times the laboratory field	[1]
β	Scatter parameter	Standard error of the slope over $\lvert b\rvert$	[1]
Q	Quality factor	Combines several parameters	[1]
VDS	Vector difference sum	Sum of vector differences of sequential demagnetization steps	[3]
$F_{\rm vds}$	Fraction of the total NRM	Total NRM is VDS	[2]
δ_i	pTRM check	Difference between pTRM at pTRM check step at T_i	[2]
$T_{\rm max}$	Maximum blocking temperature	Highest step in calculation of $\lvert b\rvert$	[2]
DRATS	Difference RATio Sum	$\sum \delta_i$ normalized by pTRM ($T_{\rm max}$)	[2]
$N_{\rm pTRM}$	Number of pTRM checks	Below $T_{\rm max}$	[2]
Δ_i	pTRM tail check	Difference between NRM remaining after first and second zero-field steps	[2]
MD%	Percent maximum difference	100x maximum value of Δ_i/VDS	[2]
T	Orientation matrix	Matrix of sums of squares and products of demagnetization data	[3]
τ_i	Eigenvalues of **T**	$\tau_1 > \tau_2 > \tau_3$	[3]
$\mathbf{V}_i$	Eigenvectors of **T**	Best-fit direction is $\mathbf{V}_1$	[3]
MAD	Maximum angle of deviation	$\tan^{-1}(\sqrt{(\tau_2^2 + \tau_3^2)}/\tau_1)$	[4]
DANG	Deviation ANGle	Angle between origin and $\mathbf{V}_1$	[2]

[1] Coe et al. (1978), [2] Tauxe and Staudigel (2004), [3] Tauxe (1998), [4] Kirschvink (1980).

erature that describe behavior during the Thellier experiment. We found those described by Tauxe and Staudigel (2004) useful. These are defined in Table 2 (see also Fig. 2).

In this study, we have assembled the entire collection of measurements made on a total of 951 specimens of basaltic glass taken from DSDP/ODP drill cores. These data have been re-interpreted for this study in a consistent manner. The data quality range from excellent to poor, with certain holes producing excellent data and others producing no usable results. For this reason, studies reporting disappointing results from a single hole cannot be taken as representative for DSDP/ODP glasses in general.

The behavior of the entire sample collection in terms of selected parameters is summarized as cumulative distributions in Fig. 3. Considering the data set as a whole, we believe that the most critical aspects in assessing the quality of the submarine basaltic glass data are (1 & 2) the scatter about the best-fit line through the NRM-pTRM data (β), and in the vector end-point diagrams (MAD) is low, (3) whether the component used is the characteristic component (trending to the origin with a low Deviation ANGle, DANG) and (4) whether the component used constitutes a significant fraction of the NRM.

To calculate the fraction of the total NRM used in the slope calculation, we use the F_{vds} parameter of Tauxe and Staudigel (2004), (see also Fig. 2a). The total remanence

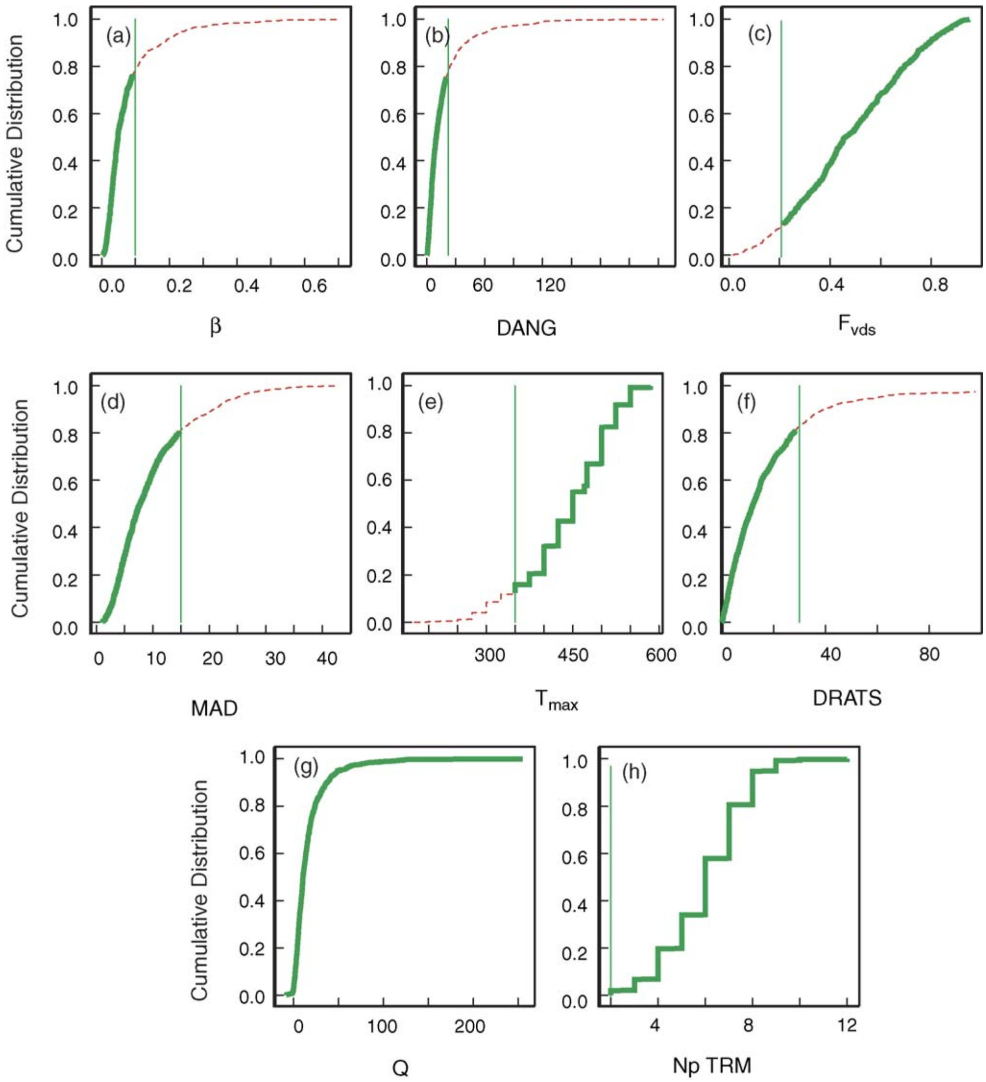

Fig. 3. Cumulative distributions of selected parameters defined in Table 2 calculated for 951 specimens of DSDP/ODP submarine basaltic glass. Vertical lines indicate cutoffs for acceptability where the solid curves are those accepted and the dashed curves are rejected.

is estimated by summing the vector difference between subsequent demagnetization steps (the vector difference sum (VDS) of, e.g., Tauxe, 1998). VDS is preferable to, say, initial NRM intensity because if there are two opposing components, the NRM intensity is much reduced being the sum of the two. VDS "straightens out" the different components to give a better estimate of the initial state. F_{vds} so defined is different from the f parameter of Coe (Coe, 1967b) because Coe's f is the fraction of only the magnetic component used in the calculation and does not take into account the possibility of multiple components of NRM. A large value of f could in fact be an insignificant fraction of the NRM if the component used is a small fraction of the NRM (see for example, Fig. 2a in which the F_{vds} is 0.2 but the f is 0.4. While this is completely unimportant in single component magnetizations, it becomes very important in specimens with several components, a frequent occurrence in older material. It is impossible to even know of the existence of multiple components with f, while F_{vds} alerts potential users of the data to the fact that the slope is based on a small fraction of the initial NRM.

T_{max} is the maximum blocking untemperature and must be sufficiently high to avoid contamination by VRM of the remanence measured. It is well known that low unblocking temperatures can be associated with low relaxation times which are also most likely to have been reset in the Brunhes Chron (see e.g., Pullaiah et al., 1975; Tauxe and Love, 2003). For example, for magnetite, blocking temperatures of less than about 225° have relaxation times of less than one million years, hence are likely to be dominated by a Brunhes age viscous magnetization and should be viewed with caution (e.g., see Thomas et al. (2004)).

For the purposes of this study, we have set the β, MAD, DANG and F_{vds} parameters at the rather conservative values of 0.1, 15°, 15° and 0.2 respectively. DRATS was set to 30% and T_{max} to 350 °C. The cutoff values for these are shown as the solid (accepted) and dotted (rejected) lines in Fig. 3. An example of the "worst" data meeting these minimum criteria is shown in Fig. 2d. In all, 504 specimens out of the original 951 experiments from the published and new data sets met these criteria. This is a success rate of 52%. A much greater success rate (151 out of 225 or 67%) was achieved in the new data presented in this paper because of better experimental design and improved equipment.

At this point, we wish to combine data that quenched under the same geomagnetic field state to calculate what in most studies would be a paleomagnetic "site" average. It is actually quite difficult to know exactly which specimens taken from a drill core should be grouped together. We have taken the DSDP/ODP concept of a "piece" as the definition of "cooling unit". A "piece" is a contiguous chunk of material that survived intact through the drilling process. These are usually separated during curation with styrofoam blocks. Their original relationship to neighboring pieces is usually unclear, although we assume that we know the relative stratigraphic order. We call individual pieces "samples" for the purpose of this paper. So for the present study, we simply average multiple specimens from the same piece to estimate sample averages. These we consider as separate cooling units.

Most studies use the standard deviation expressed as the percent of the cooling unit mean as a criterion for acceptance. This parameter is biased against low values. Alternatively, we could require that the data meet some specified target for the standard deviation, yet this would bias against higher values. We therefore follow Tauxe and Staudigel (2004) and require samples to have at least two specimens per sample and have either standard deviations ≤ 5 mT or 15% or the mean. A total of 123 samples met these criteria.

3. Results

3.1. Habitat of successful paleointensity experiments

One reason for compiling all the data from DSDP/ODP glasses together was to attempt to characterize what kinds of drill holes led to successful experiments. To this end we plot cumulative distributions of the depths (Fig. 4a) and ages (Fig. 4b) of successful (heavy lines) and unsuccessful (light dashed lines) paleointensity experiments. In general, we had slightly better success with shallower, younger specimens than with deeper, older ones. Nonetheless, usable data were obtained through out the age and depth range sampled.

3.2. Dipole moment calculation

The magnetic field of a dipole varies in magnitude by a factor of two from the equator to the pole. Therefore, to compare intensity data from different latitudes, we must convert them to some value that is independent of latitude. Using the fact that the magnetic field also varies in inclination with latitude, Thellier and Thellier (1959) normalized intensity data to a reference inclination of 65°, using the paleomagnetically determined inclination and the relationship between inclination and field strength. Doell and Cox (1961) suggested instead to normalize intensity data to a reference geographic location (50°N, 5°E). Both of these methods assume that the

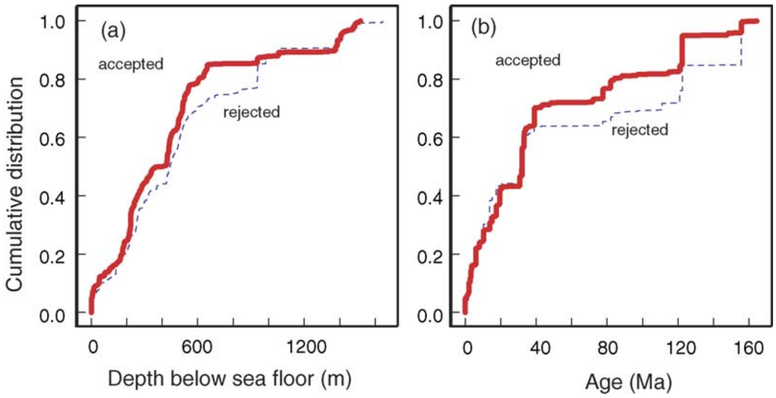

Fig. 4. Cumulative distributions of depth below sea floor (a) and age (b) of accepted (solid) and rejected (dashed) specimens.

best-fitting dipole term of the geomagnetic field has been fixed over the time of observation. Others (e.g., Nagata et al., 1963) normalized the observed intensity by the intensity at the sampling site. This latter approach suffers from the fact that the field has changed appreciably over the decades of paleointensity experiments making it problematic to compare exactly results obtained in the late 50s with those obtained today.

Noting the difficulties with all these ways of reducing paleointensity data to remove the effect of latitude, Smith (1967) argued in favor of the so-called virtual dipole moment (VDM) which is the dipole moment at the center of the Earth that would give rise to the observed intensity at the magnetic latitude of the site. The magnetic latitude λ_m is obtained from the inclination I using the well-known dipole formula ($\tan I = 2 \tan \lambda_m$). The VDM calculation, like that of the Thellier and Thellier (1959) reduced field strength calculation, requires an accurate estimate for the paleofield inclination of the sample as well as the intensity, information that is lacking in many archeological materials and our unoriented glass specimens. The VDM calculation was proposed by Smith (1967) partly because much of the variation in intensity observed in the archeomagnetic record was thought to result from movements of the dipole (so-called "dipole wobble") which would be reflected in the inclination as well as the intensity.

An alternative normalization scheme (e.g., Barbetti et al., 1977 is to calculate a virtual axial dipole moment (VADM). This is the moment of a geocentric axial dipole that would give rise to the observed intensity at the geographic latitude of the observation. In ancient times (say, older than about 5 Ma), an accurate estimate for paleolatitude (λ') is necessary for the VADM calculation.

Most data compilations have opted for the VDM calculation. Juarez et al. (1998) and Selkin and Tauxe (2000) argued that estimates for paleolatitude derived from a robust paleogeographic reconstruction model give more consistent dipole moments than the VDM calculation which relies on the less well determined "magnetic latitude" obtained from the inclination of a given observation. We follow their approach in calculating VADMs for all data compiled here. However, we have used an updated set of reference poles to re-evaluate paleolatitudes for many of the sites listed in Table 1.

Given the age, present location, and the tectonic plate for each drill site listed in Table 1, it is possible to calculate an expected direction from reference paleomagnetic poles and then the paleolatitude from the predicted inclination. This assumes that the reference poles are correct, that the magnetic field was essentially dipolar and that the age information is sufficiently accurate.

The best available reference paleomagnetic poles for our purpose are the synthetic apparent polar wander paths of Besse and Courtillot (2002). Besse and Courtillot (2002) combined data from around the globe for which the ages and finite rotations were reasonably well constrained to produce a global apparent polar wander path (APWP). This global path was then "exported" to a variety of plates as synthetic APWPs with poles estimated at 10 million year intervals. Here, we use these synthetic APWP as reference poles to estimate paleolatitude for most of the sites listed in Table 1. In this way, we are essentially using an average magnetic latitude instead of an instantaneous one. Hence, the dipole moment calculation is only really a VADM if the paleomagnetic pole was coincident with the spin axis (i.e., there was no true polar wander). Nonetheless, we refer to the dipole moments calculated here as "VADMs" in the following.

The finite rotations linking the Pacific plate to the other plates are the least well constrained. Therefore, for the Pacific drill sites that are younger than 43 Ma (the approximate age of the Hawaii-Emporor bend), we used a nominal latitudinal shift of 0.4°/m.y. Lee and Lawver

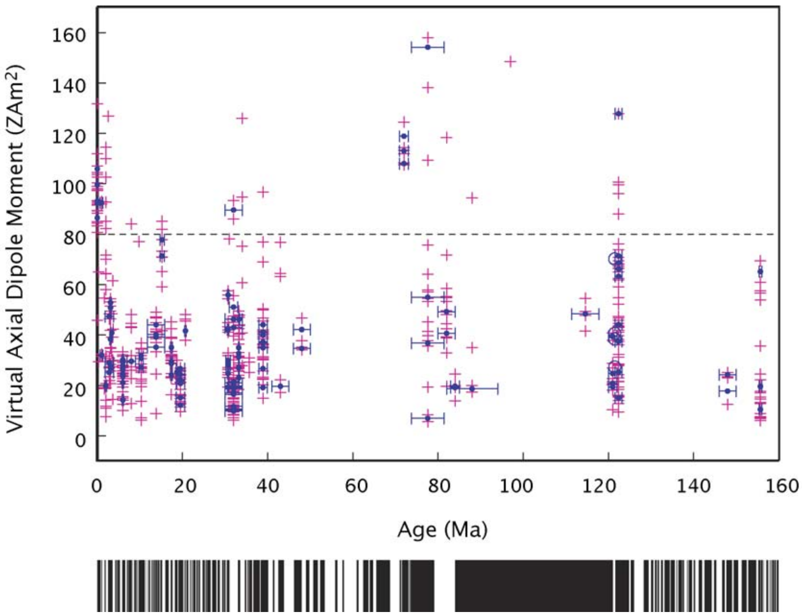

Fig. 5. Virtual axial dipole moments ($Z = 10^{21}$) for all specimens (+) and sample averages (dots) meeting minimum criteria for the submarine basaltic glass data compiled here. Also shown are the data of Riisager et al. (2003) from Site 1185. Sample data are listed in Table 3.

(1995) reconstructed the south-east Asian plate motions with respect to stable Eurasia. We used these reconstructed locations in conjunction with the European synthetic APWP to estimate λ' for DSDP Sites 447, 448 and 770. For certain sites in very old Pacific crust, we relied on paleolatitudes estimated from the average inclination data from the sites themselves (for specific references, see Table 1).

Paleolatitudes listed in Table 1 were used in the VADM calculations in this study. These are plotted in Fig. 5) with specimens as plus signs and sample averages meeting the minimum criteria for acceptance as dots (see also Table 3). Also included for completeness in Fig. 5 (as open circles) are the data of Riisager et al. (2003) from ODP Site 1185. The pattern of paleointensity variations with age is quite similar to that published by Juarez et al. (1998) and Selkin and Tauxe (2000). However, those compilations relied on data from single specimens, or site averages. In the following, we will use cooling unit (sample) averages which meet similar reproducibility requirements we have applied to the non-submarine basaltic glass data in previous publications (e.g., Tauxe and Staudigel, 2004).

3.3. The MagIC database

The Magnetics Information Consortium (MagIC) (http://earthref.org) is in the process of designing a database for all paleomagnetic and rock magnetic data. In the interest of furthering the effort on data sharing and transparency of interpretation, all the DSDP/ODP glass paleointensity data have been placed in the database. The data and meta-data are entered in a number of tables. Because there are several databases under construction at earthref.org, some of the tables are common to all databases while others are database specific. The MagIC tables are classified into several major groups: ER, PMAG, RMAG and MAGIC. Those with the prefix "ER_" are common too all earthref databases. The MagIC database is designed for both rock magnetic data ("RMAG_" tables) and paleomagnetic data ("PMAG_" tables) but there are also tables common to both types of data such as instrument and method description tables, which have the prefix "MAGIC_".

Because the notion of "location", "site" and "sample" depend on context, the choice of table and meta-data name may at times be confusing. Here, we have tried to use the most appropriate term on the basis of function. The "earthref" tables and their functions as used in this study are:

- ER_expedition: the Leg information.
- ER_localities: the DSDP/ODP "site" information.
- ER_sites: the DSDP/ODP "hole" information.
- ER_sample: such information as sample depth and mapping of our sample names to hole, core, section.

Table 3
Summary data for samples passing minimum selection criteria (see text)

Sample	Age	σ	N	B_{anc}	B_{σ}	VADM (ZAm^2) ± 1σ
0169x171111	148.0	2.0	2	12.1	0.6	24.3 ± 1.1
0169x171121	148.0	2.0	2	8.9	3.7	17.8 ± 7.5
0205x311p01	30.7	0.5	2	16.6	2.2	30.0 ± 4.0
0205x311p02	30.7	0.5	2	15.5	2.9	28.1 ± 5.3
0238x551xxx	32.0	2.0	2	43.0	2.5	89.6 ± 5.2
0238x552xxx	32.0	2.0	2	22.2	0.8	46.3 ± 1.7
0238x562049	32.0	2.0	2	20.7	2.3	43.0 ± 4.8
0238x572106	32.0	2.0	3	9.1	0.2	18.9 ± 0.4
0238x582104	32.0	2.0	4	7.9	0.6	16.5 ± 1.2
0238x601104	32.0	2.0	4	9.3	1.1	19.3 ± 2.3
0238x602131	32.0	2.0	2	10.1	0.8	21.0 ± 1.7
0238x604057	32.0	2.0	3	8.2	1.0	17.0 ± 2.1
0322x12c000	48.0	2.0	2	24.6	0.5	34.7 ± 0.7
0322x13c000	48.0	2.0	2	29.9	4.5	42.2 ± 6.4
0335x064091	13.8	2.0	2	20.4	1.6	39.2 ± 3.0
0335x091058	13.8	2.0	2	20.9	0.6	40.2 ± 1.2
0335x094127	13.8	2.0	3	18.2	4.9	35.2 ± 9.4
0335x133006	13.8	2.0	4	22.9	3.8	44.1 ± 7.2
0395a301p01	8.0	1.0	2	13.0	1.3	29.6 ± 3.0
0396b141028	10.3	0.5	3	14.0	0.5	31.8 ± 1.1
0396b143031	10.3	0.5	4	13.5	1.9	30.8 ± 4.4
0396b151039	10.3	0.5	3	11.9	0.6	27.2 ± 1.3
0407x464057	33.3	0.1	3	30.9	1.5	46.3 ± 2.3
0417d022p2a	121.0	1.0	2	9.4	0.4	20.9 ± 1.0
0417d022p2b	121.0	1.0	2	11.2	2.6	24.8 ± 5.7
0417d022p2d	121.0	1.0	2	11.2	1.4	24.8 ± 3.0
0417d022p2e	121.0	1.0	2	17.8	0.9	39.5 ± 2.0
0417d022p4c	121.0	1.0	2	8.7	0.8	19.4 ± 1.9
0420x141000	3.4	0.2	2	16.4	4.3	40.9 ± 10.6
0447a182119	43.0	2.0	2	9.6	1.7	19.7 ± 3.5
0458x461p9a	32.0	1.0	2	19.9	2.5	51.1 ± 6.5
0469x461p01	18.7	0.2	2	13.7	3.6	25.3 ± 6.7
0470a085075	15.2	0.5	4	39.4	3.4	77.8 ± 6.8
0470a131039	15.2	0.5	3	36.1	3.2	71.4 ± 6.4
0474a463000	3.1	0.2	2	24.8	1.0	52.9 ± 2.1
0474a483p01	3.1	0.2	2	18.0	2.3	38.4 ± 4.9
0474a484p09	3.1	0.2	2	13.0	4.6	27.7 ± 9.8
0474a491000	3.1	0.2	2	12.6	0.8	27.0 ± 1.8
0474a492p04	3.1	0.2	2	23.8	1.5	50.9 ± 3.3
0483b121000	2.0	0.2	2	9.3	0.5	19.9 ± 1.1
0495x483p03	20.7	0.2	2	16.2	2.1	41.7 ± 5.4
0525a005p6b	72.0	1.0	2	68.2	4.5	118.9 ± 7.9
0525a592p3h	72.0	1.0	2	61.9	0.3	108.0 ± 0.5
0525a594p1r	72.0	1.0	2	64.8	1.0	113.1 ± 1.7
0543a132p03	84.0	1.0	2	8.5	3.3	19.2 ± 7.5
0543a152p3a	84.0	1.0	2	8.6	0.2	19.7 ± 0.5
0556x041091	30.7	0.2	3	9.9	0.0	19.3 ± 0.0
0556x051116	30.7	0.2	3	21.6	0.6	42.2 ± 1.1
0556x052084	30.7	0.2	2	12.7	1.2	24.8 ± 2.3
0556x062055	30.7	0.2	3	28.7	0.8	55.9 ± 1.6
0559a073011	32.0	1.1	3	10.5	0.7	21.5 ± 1.4
0562x011p05	17.4	0.2	2	11.5	5.2	24.2 ± 11.0
0562x012114	17.4	0.2	3	13.6	1.7	28.7 ± 3.5
0562x013p3f	17.4	0.2	2	16.6	2.7	35.1 ± 5.8
0562x033113	17.4	0.2	2	14.0	0.4	29.5 ± 0.8
0564x012117	33.2	0.1	2	13.1	2.8	27.0 ± 5.7
0564x043075	33.2	0.1	5	15.9	3.6	32.7 ± 7.4
0564x071076	33.2	0.1	2	11.2	0.1	23.0 ± 0.1
0564x081101	33.2	0.1	2	15.3	0.1	31.4 ± 0.3
0564x093p02	33.2	0.1	2	17.0	2.3	35.0 ± 4.7
0706c021093	32.0	2.0	2	5.6	0.6	10.3 ± 1.1

Table 3 (*Continued*)

Sample	Age	σ	N	B_{anc}	B_{σ}	VADM (ZAm^2) $\pm 1\sigma$
0706c022039	32.0	2.0	2	10.9	5.3	19.9 ± 9.7
0706c022095	32.0	2.0	4	6.4	1.0	11.7 ± 1.8
0706c052103	32.0	2.0	3	5.4	1.8	9.9 ± 3.2
0706c053044	32.0	2.0	2	5.8	1.9	10.7 ± 3.4
0706c077010	32.0	2.0	2	5.7	1.5	10.5 ± 2.7
0758a702052	82.0	2.0	2	26.4	1.7	40.7 ± 2.6
0758a714093	82.0	2.0	3	32.0	3.6	49.3 ± 5.5
0765c631004	155.7	0.3	2	6.0	2.3	10.5 ± 4.0
0765c631088	155.7	0.3	2	11.2	4.0	19.6 ± 6.9
0765d131101	155.7	0.3	2	11.3	2.2	19.7 ± 3.8
0765d131105	155.7	0.3	2	37.4	3.4	65.2 ± 6.0
0770b173147	38.9	1.0	4	14.7	1.1	35.1 ± 2.5
0770b182035	38.9	1.0	2	15.6	1.3	37.1 ± 3.1
0770b183005	38.9	1.0	6	14.7	3.8	35.0 ± 9.0
0770c023008	38.9	1.0	2	16.8	0.8	40.0 ± 2.0
0770c023009	38.9	1.0	2	17.3	0.5	41.2 ± 1.2
0770c023019	38.9	1.0	2	15.7	1.2	37.3 ± 2.8
0770c023020	38.9	1.0	2	18.5	1.6	44.1 ± 3.8
0770c041016	38.9	1.0	2	11.2	2.0	26.7 ± 4.8
0770c04x014	38.9	1.0	3	8.1	1.6	19.2 ± 3.9
0802a582101	114.6	3.2	4	21.6	2.4	48.4 ± 5.4
0803d702120	88.0	6.0	2	9.9	1.0	18.7 ± 1.8
0807c742027	122.4	0.8	2	35.7	0.8	66.2 ± 1.6
0807c742091	122.4	0.8	2	37.0	1.7	68.6 ± 3.1
0807c742097	122.4	0.8	2	8.1	0.8	15.1 ± 1.5
0807c752004	122.4	0.8	3	34.1	2.4	63.3 ± 4.5
0807c752032	122.4	0.8	2	23.9	2.4	44.2 ± 4.4
0807c771035	122.4	0.8	2	68.9	0.0	127.8 ± 0.0
0807c791058	122.4	0.8	2	38.5	3.7	71.4 ± 6.9
0807c861105	122.4	0.8	3	20.2	2.6	37.5 ± 4.9
0807c871048	122.4	0.8	2	13.6	4.6	25.3 ± 8.5
0834b141032	6.0	0.2	4	13.4	1.0	30.2 ± 2.2
0834b152056	6.0	0.2	5	11.0	0.9	24.7 ± 2.0
0834b161047	6.0	0.2	2	10.7	0.3	24.0 ± 0.8
0834b162022	6.0	0.2	4	6.4	0.6	14.3 ± 1.3
0834b201041	6.0	0.2	4	10.5	1.6	23.7 ± 3.6
0834b261036	6.0	0.2	2	12.4	0.0	27.9 ± 0.1
0834b312047	6.0	0.2	2	13.1	0.2	29.4 ± 0.4
0834b331003	6.0	0.2	2	11.8	0.3	26.5 ± 0.7
0834b361010	6.0	0.2	2	9.4	0.3	21.1 ± 0.7
0835b041083	2.8	1.0	2	21.1	0.6	47.4 ± 1.4
0836a037073	1.0	0.3	2	14.4	0.3	32.0 ± 0.8
0836b091100	1.0	0.3	2	41.7	0.3	92.5 ± 0.7
0843a022042	97.0	5.0	3	75.8	11.2	176.6 ± 26.1
0862a031011	2.8	1.0	2	15.7	1.5	25.2 ± 2.5
0862a031098	2.8	1.0	2	18.2	1.5	29.1 ± 2.3
0864a012050	0.0	0.1	5	37.4	3.2	92.3 ± 8.0
0864a013015	0.0	0.1	5	42.9	6.4	105.9 ± 15.8
0864a015015	0.0	0.1	4	35.0	2.2	86.5 ± 5.3
0864a016030	0.0	0.1	2	37.7	2.3	93.2 ± 5.7
0864a016143	0.0	0.1	4	40.4	4.0	99.7 ± 9.9
0907a251028	19.5	1.0	2	18.0	0.1	24.4 ± 0.1
0907a254049	19.5	1.0	3	19.6	0.3	26.7 ± 0.5
0907a261053	19.5	1.0	4	16.2	1.0	21.9 ± 1.3
0907a261139	19.5	1.0	5	11.2	1.2	15.2 ± 1.6
0907a261143	19.5	1.0	5	9.0	1.2	12.2 ± 1.6
0907a262014	19.5	1.0	4	16.4	2.2	22.2 ± 2.9
0907a262019	19.5	1.0	2	15.3	2.4	20.8 ± 3.3
1001a541073	77.6	3.8	2	3.3	0.9	7.0 ± 2.0
1001a553015	77.6	3.8	2	17.2	0.7	36.8 ± 1.5
1001a561016	77.6	3.8	2	72.2	10.7	154.2 ± 22.8
1001a562026	77.6	3.8	4	25.7	3.7	55.0 ± 7.9

- ER_ages: the basement age constraints for each hole.
- ER_citations: relevant references.
- ER_mailinglist: contact information.

The "paleomagnetic" tables used here are:

- PMAG_specimens. The measurement data have been analyzed and interpreted to yield a paleofield estimate and the attendent "quality" parameters according to the procedure described in the methods section of this paper. This is the table that contains the interpretations for each specimen.
- PMAG_samples. Where possible, multiple chips were measured from a single piece. The acceptable paleofield estimates from each specimen are averaged and the data are placed in this table, including a "PMAG_criteria" meta-data code for how "acceptable" was defined.
- PMAG_sites. Here, we put hole averages of "acceptable" samples and the associated number of specimens, standard deviation, etc.
- PMAG_results. This table was designed for study average data.
- PMAG_criteria. This table contains descriptions of the definitions for acceptability. Here, we have put the specimen and sample definitions used in this study.

The MAGIC data tables used in this study are:

- MAGIC_measurements. The measurement data from all specimens from each hole are put in a measurement files with the name of magic_measurements.txt
- MAGIC_methods. There are places throughout all the RMAG and PMAG tables for so-called "method codes". These describe field, sample preparation, laboratory protocols, statistical analyses and the like. The definitions for each code and the relevant citations are put in the methods table.
- MAGIC_instruments. Each instrument used in the study has been named and described in this table. Instrument codes are used in the measurements table, attached to the appropriate measurement.

Data, meta data and interpretations for 951 specimens of submarine basaltic glass (both published and new) have been assembled in a uniform naming and data interpretation scheme. These data have been put into MagIC formatted tab delimited files and have been submitted to the Earthref.org database.

4. Discussion

4.1. Comparision of DSDP/ODP submarine basaltic glass data with other published data

Paleointensity data have been published for over five decades. Many of these data have been compiled in the so-called PINT database initiated by Tanaka et al. (1995) and currently maintained by Perrin et al. (1998). We use the compilation of data of Tauxe and Staudigel (2004) (available at http://earthref.org). Their compilation includes data from 1–160 Ma published through early 2004 that were obtained from Thellier–Thellier experiments (with pTRM checks). They excluded explicitly transitional data and data for sites with only one specimen. They further required sites to meet the standard deviation of ≤ 5 mT or 15% of the mean as a criterion as in the glass data. There are data from 209 cooling units in this dataset. VADMs were calculated for each of these paleointensity estimates using model latitudes derived from Besse and Courtillot (2002) for consistency with the glass data. We plot these VADMs as triangles in Fig. 6. Those from the Troodos submarine basaltic glass data are shown as filled triangles while the rest of the data compilation (mostly lava flow data) are open triangles. The sample averages of DSDP/ODP glasses from Fig. 5 are shown as dots.

4.2. Average dipole moment and trends

Now we may address the issue of the "average value" of the geomagnetic field intensity raised in the introduction. In Fig. 7 we plot a histogram of the data shown in Fig. 6. The data are clearly not normally distributed, but have a long, high-VADM tail. The present day value of about 80 ZAm^2 is much larger than the bulk of the data the mode of which is about 40 ZAm^2.

4.3. Comparison of lava flow and glass data sets

The distribution of data from the submarine basaltic glass is different from those derived from non-glass materials (see Fig. 8) with the lava flow data being some 20% higher on average than the SBG data. Possible reasons for the difference include:

(1) Contribution of transitional data in the glasses: We explicitly rejected all lava flow data labelled as "transitional" in the publications or databases but cannot do so in the unoriented glass data. Because transitional data are almost always very low intensity, it is

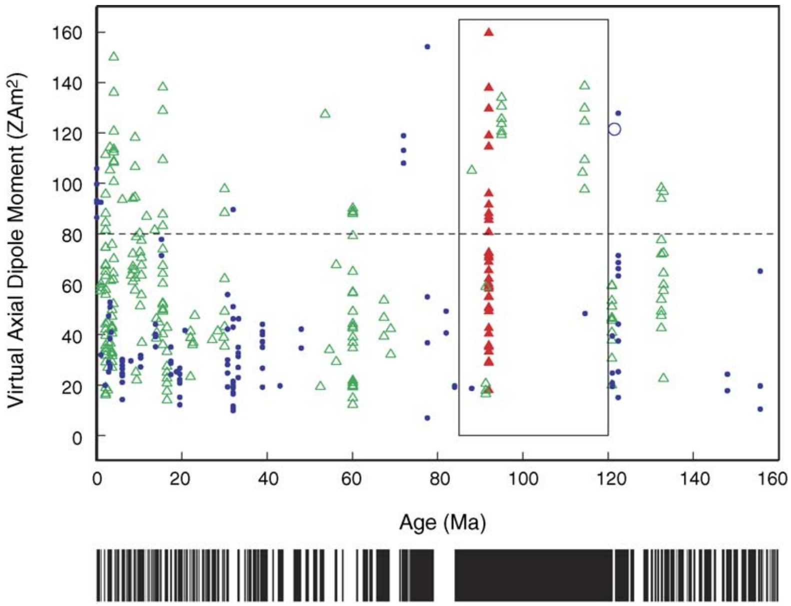

Fig. 6. Summary of VADM data versus age. Triangles are from the published literature compiled by Tauxe and Staudigel (2004) (those in red are the Troodos submarine basaltic glass data). Dots are the sample averages from Fig. 5. The present field is the dotted line. The thin solid line is the average dipole moment calculated assuming a log-normal distribution (see text). At the bottom is the Geomagnetic Polarity Time scale from Berggren et al. (1995) and Gradstein et al. (1995) used here.

possible that their exclusion from one data set and inclusion in the other could produce a bias. However, this is unlikely to have a big effect because the field is only in rarely in a state of reversal and the glass data do not target reversals as the lava flow studies have tended to do. Morever, the "floor" in intensity appears to be the same in both the glass and the lava flow data ($\sim$10 ZAm^2; see Fig. 6).

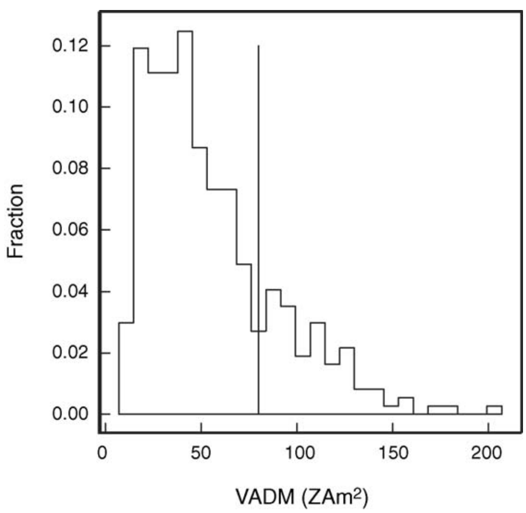

Fig. 7. Histogram of all data shown in Fig. 6. The present day value is the vertical line. The data are clearly not normally distributed, but have a long high intensity tail.

(2) Difference in experimental design: The main difference between the two largest data sets in Fig. 6 (lava flows and SBG data) is that there are many more high values in the lava flow data than in the SBG data. Many of lava flow data come from studies with adequate experimental control (e.g., Prévot et al., 1985; Bogue and Paul, 1993; Goguitchaichvili et al., 2002), yet very few include the pTRM-tail check of Riisager and Riisager (2001). It is therefore possible, if not in fact likely, that some of the lava flow data are affected by the concave downward NRM-pTRM curves that are associated with undemagnetized pTRM tails. Concave downward curves have the effect of generating a bias toward high values. The initial slope of the NRM-pTRM plots are most often chosen because the samples have not yet altered, and are often biased high by the pTRM tails. SBG does not suffer from this problem, because the remanence is carried by single domain magnetite (see e.g., Tauxe and Staudigel, 2004; Tauxe et al., 1996).

(3) Different ages of the different data sets: The lava flow data and the glass data rarely come from exactly the same polarity intervals. The exception to this is the CNS where ironically the glass data have

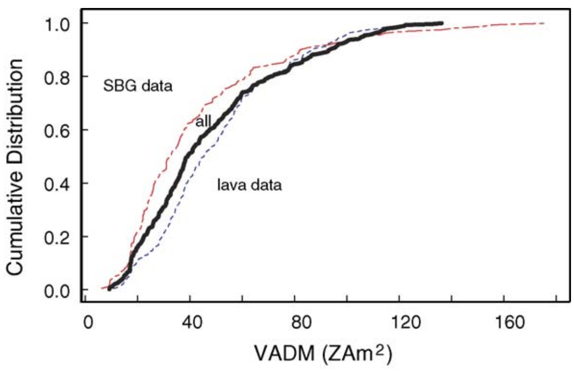

Fig. 8. Cumulative distributions of the VADM data from Fig. 6.

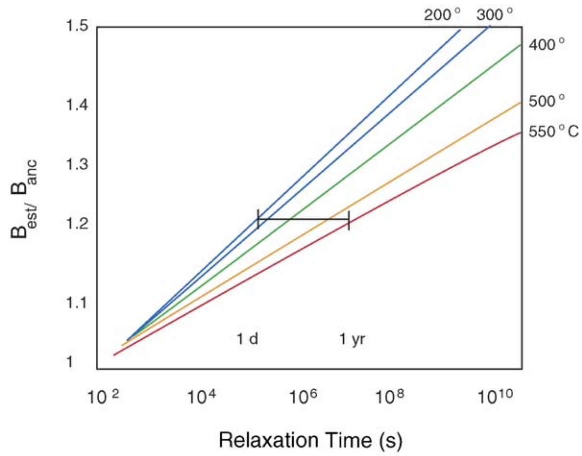

Fig. 9. Theoretical effect of cooling rate on estimated paleointensity (B_{est}) relative to the ancient field B_{anc} as a function of relaxation time. The slower the cooling rate, the longer the effective relaxation time. The relaxation time during laboratory experiments is assumed to be approximately 100 s. The temperature labels for each line are blocking temperatures. A 20% difference between lava flow data and SBG could be caused if the lava flow cooled to about 400 °C over a period of days to months. (Figure redrawn from Selkin et al., 2000, see also Halgedahl et al., 1980.)

higher intensity values than the lava flow data. So it is possible that the larger lava flow data set sampled intervals with high fields that were not sampled by the glasses.

(4) Different cooling rates: It is well known that lava flows cool more slowly than quenched glasses and may take days or years to cool in their interiors. It is also well known that the ratio of original cooling rate to laboratory cooling rate has a profound influence on the paleofield calculation (e.g., Fox and Aitken, 1980). The slower the original cooling and the lower the blocking temperature, the larger the over estimate of the field (see Fig. 9). To explain the 20% difference in means between datasets using the cooling rate effect, we would require that on average, lava flow samples originally cooled to about 400 °C in less than 10 days. Such a scenario is entirely possible and may be a major cause for the discrepancy between lava flow and glass data.

4.4. Polarity interval length and paleointensity

Although there are no clear long-term trends in the paleointensity data, there are times when the field is stronger than others, for example in the Cretaceous Normal Superchron (CNS; box in Fig. 6) and the Brunhes. It has long been suggested that strong fields would suppress the tendency of the geomagnetic field to reverse (e.g. Cox, 1968). The relative paleointensity data from DSDP Site 522 (e.g, Tauxe and Hartl, 1997) showed a weak correlation between polarity interval length and paleofield strength, a finding that supported Cox's hypothesis. One of the primary motivations for initiating the study of the DSDP/ODP submarine basaltic glasses for paleointensity therefore was to test the hypothesis that long intervals of stable polarity (like the Cretaceous Normal Superchron or CNS in Fig. 6) were associated with unusually strong fields (e.g., Pick and Tauxe, 1993b). So it came as somewhat of a surprise when Selkin and Tauxe (2000) compared paleofield strength with reversal rate and concluded that there was no clear relationship. Until the work of Tauxe and Staudigel (2004), there were simply too few data within the CNS itself to make a robust paleofield estimate. Glasses from the Troodos Ophiolite (shown as filled triangles in Fig. 6) showed that the average VADM during the CNS was quite similar to today's dipole moment (shown as the dashed line in Fig. 6). Yet, there remains no convincing trend of decreasing field strength toward the present with the generally accepted increase in the rate of reversals.

On reflection, a correlation between polarity interval length and average field strength does not require a dependence of field strength on reversal rate. A slow rate of reversals, like during the Paleogene, has many intervals of quite short duration interspersed with periods of unusually long duration. Therefore, what is required to test the Cox hypothesis is a sufficient number of paleointensity estimates (at least 20 according to the Monte Carlo simulations of Tauxe and Staudigel, 2004) which are unambiguously tied to particular polarity interval of known duration, a rare occurrence in the paleointensity database in general.

The CNS is of sufficient duration that the assignment of data to it is very straight-forward. The CNS data were compiled by Tauxe and Staudigel (2004) as already mentioned. Riisager and Abrahamsen (2000) report paleointensity data from a sequence of lava flows with a magnetostratigraphic pattern tied to C27n-C26r. They note an asymmetry in intensity with a low field (16 μT) during C27n compared to 43.3 μT during C26r. They suggest that the strong C26r field is "post-transitional" and that the asymmetry was an inherent process of reversals. We suggest instead that the asymmetry results from the fact that C26r is quite a long polarity interval (approximately 3 m.y) compared to C27n, which is quite short (about one tenth the duration). Finally, most DSDP/ODP sites are loosely associated with magnetic anomaly data (see e.g., Fig. 1), and several are securely tied to a particular polarity interval (although none of these have as many as 20 samples).

In Fig. 10 we plot the data compiled by Tauxe and Staudigel (2004) for the CNS and the Greenland lava flow data of Riisager and Abrahamsen (2000) (C26r, C27n). Single crystal data (Tarduno et al., 2001, 2002) are plotted as squares. We plot the Brunhes data compiled by Tauxe and Love (2003) as solid triangles. The circles are the "zero age" data from Site 864. Also shown are the accepted data from the present study obtained from each hole with well controlled anomaly identifications. It appears that the correlation suggested by Tauxe and Hartl (1997) based on relative paleointensity in sediments is supported by the absolute paleointensity data set as well.

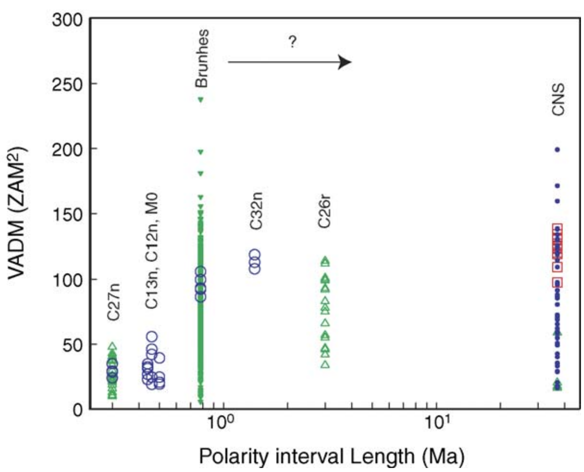

Fig. 10. Data from the present study (open and closed circles); the compilation of Tauxe and Staudigel (2004) (open triangles and squares) and the Brunhes compilation of Tauxe and Love (2003) (solid triangles). The associated polarity chrons are noted.

Some have suggested that because the magnetic field has dropped in intensity quite rapidly over the recent past (e.g., Hulot et al., 2002) that we may be headed toward a reversal. The Brunhes VADM data are as strong (if not stronger) than those from the CNS and the present field is about twice the average. Yet, we do not yet know its duration (as it has not yet finished!). Because field strength appears to be related to polarity interval length, it is possible that instead of heading for reversal, we may have to wait a long time for it instead.

5. Conclusions

- We have compiled paleointensity data from 951 specimens obtained from DSDP/ODP submarine basaltic glass material. These data have been contributed to the Magnetics Information Consortium (MagIC) database found at http://earthref.org. An ascii file of the entire MagIC template file has also been provided as supplemental material.
- The data set compiled here includes 225 new experiments carried out in order to augment the number of samples with replicate measurements. These experiments were done using the IZZI protocol of Tauxe and Staudigel (2004) and Yu et al. (2004) whereby infield-zero-field (IZ) measurements are alternated with zero-field-infield (ZI) measurements in the Thellier–Thellier paleointensity experiment. The IZZI protocol reveals non-ideal behavior resulting from the inequality of blocking and unblocking temperatures, obviating the need for a second zero field step after the infield step proposed by for example Riisager and Riisager (2001).
- All published and new submarine basaltic glass data available to us from DSDP/ODP holes were (re)analyzed in a consistent fashion. Specimen data meeting minimum acceptance criteria were averaged together by sample. 123 samples spanning the age range from zero age to nearly 160 Ma are considered to be reliable.
- We combined data from the DSDP/ODP glasses with what we consider to be the most reliable published data. Submarine basaltic glass data (including 39 cooling unit averages from the Troodos Ophiolite) represent approximately 44% of the entire paleointensity data base. The data set taken as a whole support the conclusions of Selkin and Tauxe (2000) that (1) the present (∼80 ZAm^2) and recent geomagnetic dipole intensity (up to perhaps ∼120 ZAm^2) is substantially stronger than the average field strength and that (2) the Mesozoic dipole low of e.g., Prévot et al. (1990) is not "low", but of average field strength.

- There has been a long-standing paradox that while Tauxe and Hartl (1997) found a weak correlation between average field strength and polarity interval length in their relative paleointensity data from the Oligocene record of DSDP Site 522, no significant trend suggesting higher field strengths with lower reversal rate has ever been convincingly demonstrated. We find in this study that when absolute paleointensity data can be securely tied to a particular polarity interval (so that polarity interval length is well constrained), there does appear to be a relationship between interval length and average field strength. The solution to the paradox is that periods of slow reversal rate are characterized by long polarity intervals, punctuated by short polarity intervals. Data from the short polarity intervals (with lower average values) may obscure the fact that the long polarity intervals have higher average values.
- Paleointensity data from the Brunhes are as strong and variable as those from the Cretaceous Normal Superchron. We do not yet know the length of the Brunhes, but taking the relationship between average field strength and polarity interval length at face value, we suggest that instead of racing toward a polarity reversal (e.g., Hulot et al., 2002), we may instead be living in the midst of an unusually long period of polarity stability.

Acknowledgements

I would like to acknowledge the collaboration of Thomas Pick, Teresa Juarez, and Peter Selkin in the original work on submarine basaltic glass. I am grateful for many useful conversations with Jeff Gee, Julie Bowles, and Cathy Constable. Jason Steindorf made the measurements for the new data presented in this study. Philip Staudigel helped to put the MagIC database together. Anthony Koppers did the heavy lifting designing the MagIC database. This work was partially supported by NSF grants 0003395 and 0229498 to LT.

References

Barbetti, M., McElhinny, M., Edwards, D., Schmidt, P., 1977. Weathering processes in baked sediments and their effects on archaeomagnetic field-intensity measurements. Phys. Earth Planet. Int. 13, 346–354.

Berggren, W., Kent, D., Swisher III, C., Aubry, M.-P., 1995. A revised Cenozoic geochronology and chronostratigraphy. In: Berggren, W., Kent, D., Aubry, M.-P., Hardenbol, J. (Eds.), Geochronology Time Scales and Global Stratigraphic Correlation. SEPM, Tulsa, Oklahoma, pp. 129–212.

Besse, J., Courtillot, V., 2002. Apparent and true polar wander and the geometry of the geomagnetic field over the last 200 Myr. J. Geophys. Res. 107 (B11), 2300, doi:10.1029/2000JB000050.

Biggin, A.J., Thomas, D.N., 2003. Analysis of long-term variations in the geomagnetic poloidal field intensity and evaluation of their relationship with global geodynamics. Geophys. J. Int. 152 (2), 392–415.

Bogue, S., Paul, H., 1993. Distinctive field behavior following geomagnetic reversals. Geophys. Res. Lett. 20, 2399–2402.

Bol'shakov, A., Solodovnikov, G.M., 1980. Paleomagnetic data on the intensity of the magnetic field of the Earth. Izv. Earth Phys. 16, 602–614.

Bowles, J., Gee, J., Kent, D. V., Bergmanis, E., Sinton, J., 2005. Cooling rate effects on paleointensity estimates in submarine basaltic glass and implications for dating young flows. Geochem. Geophys. Geosyst. 6, Q07002, doi:10.1029/2004GC000900.

Cande, S., LaBrecque, J., Larson, R., Pitman III, W., Golovchenko, X., Haxby, W., 1989. Magnetic lineations of the world's Ocean Basins (map with text).

Carlut, J., Kent, D., 2000. Paleointensity record in zero-age submarine basalt glass: testing a new dating technique for recent MORBS. Earth Planet. Sci. Lett. 183, 389–401.

Castillo, P.R., Pringle, M.S., Carlson, R.W., 1994. East Mariana Basin Tholeiites – Cretaceous intraplate basalts of rift basalts related to the Ontong Java Plume. Earth Planet. Sci. Lett. 123 (1–4), 139–154.

Coe, R.S., 1967a. The determination of paleo-intensities of the Earth's magnetic field with emphasis on mechanisms which could cause non-ideal behavior in Thellier's method. J. Geomagn. Geoelectr. 19, 157–178.

Coe, R.S., 1967b. Paleointensities of the Earth's magnetic field determined from Tertiary and Quaternary rocks. J. Geophys. Res. 72, 3247–5281.

Coe, R.S., Grommé, S., Mankinen, E.A., 1978. Geomagnetic paleointensities from radiocarbon-dated lava flows on Hawaii and the question of the Pacific nondipole low. J. Geophys. Res. 83, 1740–1756.

Cox, A.V., 1968. Lengths of geomagnetic polarity intervals. J. Geophys. Res. 73, 3247–3260.

DeMets, C., Gordon, R.G., Argus, D.F., Stein, S., 1990. Current plate motions. Geophys. J. Int. 101, 425–478.

Doell, R., Cox, A., 1961. Paleomagnetism. Adv. Geophys. 8, 221.

Fox, J.M.W., Aitken, M.J., 1980. Cooling-rate dependence of thermoremanent magnetization. Nature 283, 462–463.

Goguitchaichvili, A., Alva-Valdivia, L., Rosas-Elguera, J., Urrutia-Fucugauchi, J., Gonzalez, J.A., Morales, J., Sole, J., 2002. An integrated paleomagnetic study of Rio Grande de Santiago volcanic succession (trans-Mexican volcanic belt): revisited. Phys. Earth Planet. Int. 130 (3–4), 175–194.

Goguitchaichvili, A., Alva-Valdivia, L.M., Luis, M., Rosas-Elguera, J., Urrutia-Fucugauchi, J., Sole, J., 2004. Absolute geomagnetic paleointensity after the cretaceous Normal Superchron and just prior to the Cretaceous-Tertiary transition. J. Geophys. Res. 109, B01105, doi:10.1029/2003JB002477.

Gradstein, F., Agterberg, F., Ogg, J., Hardenbol, J., Van Veen, P., Thierry, J., Huang, Z., 1995. A Triassic, Jurassic and Cretaceous time scale. In: Berggren, W., Kent, D., Aubry, M.-P., Hardenbol, J. (Eds.), Geochronology Time Scales and Global Stratigraphic Correlation. SEPM, Tulsa, Oklahoma, pp. 95–126.

Halgedahl, S., Day, R., Fuller, M., 1980. The effect of cooling rate on the intensity of weak-field TRM in single-domain magnetite. J. Geophys. Res. 95, 3690–3698.

Heller, R., Merrill, R.T., McFadden, P.L., 2002. The variation of intensity of earth's magnetic field with time. Phys. Earth Planet. Int. 131 (3–4), 237–249.

Hulot, G., Eymin, C., Langlais, B., Mandea, M., Olsen, N., 2002. Small-scale structure of the geodynamo inferred from Oersted and Magsat satellite data. Nature 416, 620–623.

Juarez, M., Tauxe, L., 2000. The intensity of the time averaged geomagnetic field: the last 5 Myr. Earth Planet. Sci. Lett. 175, 169–180.

Juarez, T., Tauxe, L., Gee, J.S., Pick, T., 1998. The intensity of the Earth's magnetic field over the past 160 million years. Nature 394, 878–881.

Kent, D.V., Gee, J., 1996. Magnetic alteration of zero-age oceanic basalt. Geology 24, 703–706.

Kirschvink, J.L., 1980. The least-squares line and plane and the analysis of paleomagnetic data. Geophys. J. Roy. Astron. Soc. 62, 699–718.

Kono, M., 1971. Intensity of the earth's magnetic field during the Pliocene and Pleistocene in relation to the amplitude of mid-ocean ridge magnetic anomalies. Earth Planet. Sci. Lett. 11, 10–17.

Lee, T.-Y., Lawver, L., 1995. Cenozoic plate reconstruction of Southeast asia. Tectonophysics 251, 85–138.

Mahoney, J., Storey, M., Duncan, R., Spencer, K., Pringle, M., 1993. Geochemistry and age of the Ontong-Java Plateau. In: Pringle, M., Sager, W., Sliter, W., Stein, S. (Eds.), The Mesozoic Pacific: Geology Tectonics and Volcanism. American Geophysical Union, Washington, DC, pp. 233–262.

McFadden, McElhinny, 1982. Variations in the geomagnetic dipole 2: statistical analysis of VDM's for the past 5 Myr. J. Geomagn. Geoelectr. 34, 163–189.

Mejia, V., Opdyke, N.D., Perfit, M.R., 1996. Paleomagnetic field intensity recorded in submarine basaltic glass from the East Pacific Rise, the last 69 ka. Geophys. Res. Lett. 23, 475–478.

Nagata, T., Arai, Y., Momose, K., 1963. Secular variation of the geomagnetic total force during the last 5000 years. J. Geophys. Res. 68, 5277–5282.

Nakanishi, M., Tamaki, K., Kobayashi, Y., 1992. Magnetic anomaly lineations from Late Jurassic to Early cretaceous in the west-central Pacific Ocean. Geophys. J. Int. 109, 701–719.

Perrin, M., Schnepp, E., Shcherbakov, V., 1998. Paleointensity database updated. EOS, Trans. AGU 79, 198.

Perrin, M., Shcherbakov, V., 1997. Paleointensity of the Earth's magnetic field for the past 400 ma: evidence for a dipole structure during the Mesozoic low. J. Geomagn. Geoelectr. 601–614.

Pick, T., Tauxe, L., 1993a. Geomagnetic paleointensities during the Cretaceous normal superchron measured using submarine basaltic glass. Nature 366, 238–242.

Pick, T., Tauxe, L., 1993b. Holocene paleointensities: Thellier experiments on submarine basaltic glass from the East Pacific Rise. J. Geophys. Res. 98, 17949–17964.

Pick, T., Tauxe, L., 1994. Characteristics of magnetite in submarine basaltic glass. Geophys. J. Int. 119, 116–128.

Prévot, M., Derder, M.E.M., McWilliams, M., Thompson, J., 1990. Intensity of the Earth's magnetic field: evidence for a Mesozoic dipole low. Earth Planet. Sci. Lett. 97, 129–139.

Prévot, M., Mankinen, E.A., Coe, R.S., Grommé, C.S., 1985. The Steens Mountain (Oregon) geomagnetic polarity transition 2. Field intensity variations and discussion of reversal models. J. Geophys. Res. 90, 10417–10448.

Pullaiah, G., Irving, E., Buchan, K., Dunlop, D., 1975. Magnetization changes caused by burial and uplift. Earth Planet. Sci. Lett. 28, 133–143.

Riisager, P., Abrahamsen, N., 2000. Palaeointensity of West Greenland Palaeocene basalts: asymmetric intensity around the c27n–c26r transition. Phys. Earth Planet. Int. 118 (1–2), 53–64.

Riisager, P., Riisager, J., 2001. Detecting multidomain magnetic grains in Thellier palaeointensity experiments. Phys. Earth Planet. Int. 125 (1–4), 111–117.

Riisager, P., Riisager, J., Zhao, X., Coe, R., 2003. Cretaceous geomagnetic paleointensities: Thellier experiments on pillow lavas and submarine basaltic glass from the Ontong Java Plateau. Geochem. Geophys. Geosyst. 4 (1–2), 8803, doi:10.1029/2003GC000611.

Sager, W.W., 2004. Data report: paleomagnetism of basaltic rocks cored from Western Pacific DSDP and ODP boreholes. In: Kanazawa, T., Escutia, C. (Eds.), Proc. ODP, Scientific Res, vol. 191. Ocean Drilling Program, College Station, TX, pp. 1–27.

Selkin, P., Gee, J., Tauxe, L., Meurer, W., Newell, A., 2000. The effect of remanence anisotropy on paleointensity estimates: a case study from the Archean Stillwater complex. Earth Planet. Sci. Lett. 182, 403–416.

Selkin, P., Tauxe, L., 2000. Long-term variations in paleointensity. Phil. Trans. Roy. Soc. Lond. 358, 1065–1088.

Smirnov, A.V., Tarduno, J.A., 2003. Magnetic hysteresis monitoring of Cretaceous submarine basaltic glass during Thellier paleointensity experiments: evidence for alteration and attendant low field bias. Earth Planet. Sci. Lett. 206 (3–4), 571–585.

Smith, P.J., 1967. The intensity of the ancient geomagnetic field: a review and analysis. Geophys. J. Roy. Astron. Soc. 12, 321–362.

Steiner, M.B., 1981. Paleomagnetism of the Cretaceous section, Site 462. Init. Rep. DSDP 61, 711–716.

Tanaka, H., Kono, M., Uchimura, H., 1995. Some global features of paleointensity in geological time. Geophys. J. Int. 120, 97–102.

Tarduno, J.A., Cottrell, R.D., Smirnov, A.V., 2001. High geomagnetic intensity during the mid-Cretaceous from Thellier analyses of single plagioclase crystals. Science 291 (5509), 1779–1783.

Tarduno, J.A., Cottrell, R.D., Smirnov, A.V., 2002. The Cretaceous superchron geodynamo: observations near the tangent cylinder. Proc. Natl. Acad. Sci. USA 99 (22), 14020–14025.

Tauxe, L., 1998. Paleomagnetic Principles and Practice. Kluwer Academic Publishers, Dordrecht.

Tauxe, L., Hartl, P., 1997. 11 million years of oligocene geomagnetic field behaviour. Geophys. J. Int. 128, 217–229.

Tauxe, L., Love, J., 2003. Paleointensity in Hawaiian Scientific Drilling project Hole (HSDP2): results from submarine basaltic glass. Geochem. Geophys. Geosyst. 4 (2), 8702, doi:10.1029/2001GC000276.

Tauxe, L., Mullender, T.A.T., Pick, T., 1996. Potbellies, wasp-waists, and superparamagnetism in magnetic hysteresis. J. Geophys. Res. 101, 571–583.

Tauxe, L., Staudigel, H., 2004. Strength of the geomagnetic field in the Cretaceous Normal Superchron: new data from submarine basaltic glass of the Troodos Ophiolite. Geochem. Geophys. Geosyst. 5 (2), Q02H06, doi:10.1029/2003GC000635.

Thellier, E., Thellier, O., 1959. Sur l'intensité du champ magnétique terrestre dans le passé historique et géologique. Ann. Geophys. 15, 285–378.

Thomas, D.N., Hill, M., Garcia, A., 2004. Comparison of the Coe-Thellier–Thellier and microwave paleointensity techniques using high-titanium titanomagnetites: results from a Tertiary basaltic intrusion from the Sydney Basin, New South Wales. Earth Planet. Sci. Lett. 229, 15–29.

Wallick, B., Steiner, M.B., 1992. Paleomagnetism of Cretaceous basalts from the East Mariana Basin, Western Pacific Ocean. In: Larson, R., et al. (Eds.), Proceedings of the Ocean Drilling Program, Scientific Results, vol. 129. Ocean Drilling Program, College Station, TX, pp. 447–454.

Yan, C., Kroenke, L., 1993. A plate tectonic reconstruction of the Southwest Pacific 0–100 ma. In: Berger, W., et al. (Eds.), Proceedings of the Ocean Drilling Program, Scientific Results, vol. 130. Ocean Drilling Program, College Station, TX, pp. 697–709.

Yu, Y., Tauxe, L., Genevey, A., 2004. Toward an optimal geomagnetic field intensity determination technique. Geochem. Geophys. Geosyst. 5 (2), Q02H07 doi:10.1029/2003GC000630.

Zhou, W., Van der Voo, R., Peacor, D., 1997. Single-domain and superparamagnetic titanomagneitte with variable Ti content in young ocean floor basalts: no evidence for rapid alteration. Earth Planet. Sci. Lett. 150, 353–362.